AFRL-AFOSR-VA-TR-2023-0385

LARGE ARRAYS OF MICROLASERS FOR FAR AND NEAR-FIELD IMAGING AND LIDAR IN THE INFRARED, VISIBLE, AND ULTRAVIOLET

Eden, James
UNIVERSITY OF ILLINOIS
506 S WRIGHT ST
URBANA, IL, 61801
USA

07/06/2023
Final Technical Report

Air Force Research Laboratory
Air Force Office of Scientific Research
Arlington, Virginia 22203
Air Force Materiel Command

REPORT DOCUMENTATION PAGE

PLEASE DO NOT RETURN YOUR FORM TO THE ABOVE ORGANIZATION.

1. REPORT DATE	2. REPORT TYPE	3. DATES COVERED	
20230706	Final	START DATE 20180701	END DATE 20220630

4. TITLE AND SUBTITLE
LARGE ARRAYS OF MICROLASERS FOR FAR AND NEAR-FIELD IMAGING AND LIDAR IN THE INFRARED, VISIBLE, AND ULTRAVIOLET

5a. CONTRACT NUMBER	5b. GRANT NUMBER	5c. PROGRAM ELEMENT NUMBER
	FA9550-18-1-0380	61102F
5d. PROJECT NUMBER	**5e. TASK NUMBER**	**5f. WORK UNIT NUMBER**

6. AUTHOR(S)
James Eden

7. PERFORMING ORGANIZATION NAME(S) AND ADDRESS(ES)
UNIVERSITY OF ILLINOIS
506 S WRIGHT ST
URBANA, IL 61801
USA

8. PERFORMING ORGANIZATION REPORT NUMBER

9. SPONSORING/MONITORING AGENCY NAME(S) AND ADDRESS(ES)	10. SPONSOR/MONITOR'S ACRONYM(S)	11. SPONSOR/MONITOR'S REPORT NUMBER(S)
Air Force Office of Scientific Research 875 N. Randolph St. Room 3112 Arlington, VA 22203	AFRL/AFOSR RTB1	AFRL-AFOSR-VA-TR-2023-0385

12. DISTRIBUTION/AVAILABILITY STATEMENT
A Distribution Unlimited: PB Public Release

13. SUPPLEMENTARY NOTES

14. ABSTRACT
This AFOSR grant, initiated by Dr. Gernot S. Pomrenke in 2019, has been dedicated to the development of microlaser cavities for the pursuit of optical imaging systems and LIDAR which was first demonstrated under Grant No. FA9550-14-1-0002. We are pleased to report to AFOSR that the past three years of research have proven to be quite productive, yielding several developments that appear to be of significant value to the Air Force. Highlights of this research program include

15. SUBJECT TERMS

16. SECURITY CLASSIFICATION OF:			17. LIMITATION OF ABSTRACT	18. NUMBER OF PAGES
a. REPORT	b. ABSTRACT	c. THIS PAGE		
U	U	U	UU	14

19a. NAME OF RESPONSIBLE PERSON	19b. PHONE NUMBER *(Include area code)*
JOHN LUGINSLAND	000-0000

Standard Form 298 (Rev.5/2020)
Prescribed by ANSI Std. Z39.18

FINAL PERFORMANCE REPORT
FOR AFOSR GRANT
NO. FA9550-18-1-0380

"LARGE ARRAYS OF MICROLASERS FOR FAR AND NEAR-FIELD IMAGING AND LIDAR IN THE INFRARED, VISIBLE, AND ULTRAVIOLET"

Prepared For

Dr. John Luginsland
U.S. Air Force Office of Scientific Research
One Liberty Center
875 North Randolph Street
Arlington, VA 22203-1768

Submitted By

J. Gary Eden
University of Illinois
Department of Electrical and Computer Engineering
306 North Wright Street
Urbana, IL 61801

September 2022

I. INTRODUCTION AND SUMMARY OF ACCOMPLISHMENTS

This AFOSR grant, initiated by Dr. Gernot S. Pomrenke in 2019, has been dedicated to the development of microlaser cavities for the pursuit of optical imaging systems and LIDAR which was first demonstrated under Grant No. FA9550-14-1-0002. We are pleased to report to AFOSR that the past three years of research have proven to be quite productive, yielding several developments that appear to be of significant value to the Air Force. Highlights of this research program include:

1. The conception and development of a laser whose output comprises literally thousands of microlaser beams using Ti:Al_2O_3 as the gain media. In the far field, these beams combine to form a single beam of low coherence and virtually no speckle. Such a laser has been pursued for decades by the optical community and is ideal for high spatial and temporal resolution LIDAR.
2. Speckle-free imaging at long distances, of moving objects, and of biological species.
3. Fractal Lasers
    a. Fundamental mode first observed at UIUC (described in a 2018 paper)
    b. Higher-order modes observed experimentally, and consistent with simulations

In addition to these technical accomplishments, 29 U.S. and international patents have been received during this grant. Every one of these patents acknowledges AFOSR as the sole supporter of the results being patented. Finally, technical articles have been published in high quality journals as a result of this grant. Once again, each article credits AFOSR as the source of support.

Before describing these and other accomplishments realized under AFOSR support, the PI (J.G. Eden) wishes to express his gratitude, and that of our students, to AFOSR and AFRL for the support of this work. Dr. Eden wishes to also extend his apologies for the excessive delay in submitting this report. It was actually written in 2022 but was not submitted officially on time because, in all honesty, it was forgotten. For this, we hope that AFOSR will accept our apology!

II. BRIEF DESCRIPTION OF SEVERAL HIGHLIGHTS

In this section, a few of the highlights listed above are described briefly. Details regarding these and other accomplishments can be found in the publications listed in Section III.

A. Long Distance Imaging

One of the major accomplishments realized under this AFOSR Program was the ability to use the arrays of microbeams to image from a far distance with high spatial resolution while overcoming the challenge of speckle. In panels a)-c) of Fig. 1, a comparison of three different images acquired with three different sources were taken at a distance of 3 m. In each of these images, speckle was a challenge. In this work, Ti:Al_2O_3 was used as the gain medium in a Fabry-Pérot cavity stabilized by a microlens array. Fig. 1d) was acquired at a distance of 5 m using this laser with significant speckle reduction. In addition to imaging from a long-distance, high-quality images were also obtained under less-than-ideal conditions such as fog as shown in Fig. 1e).

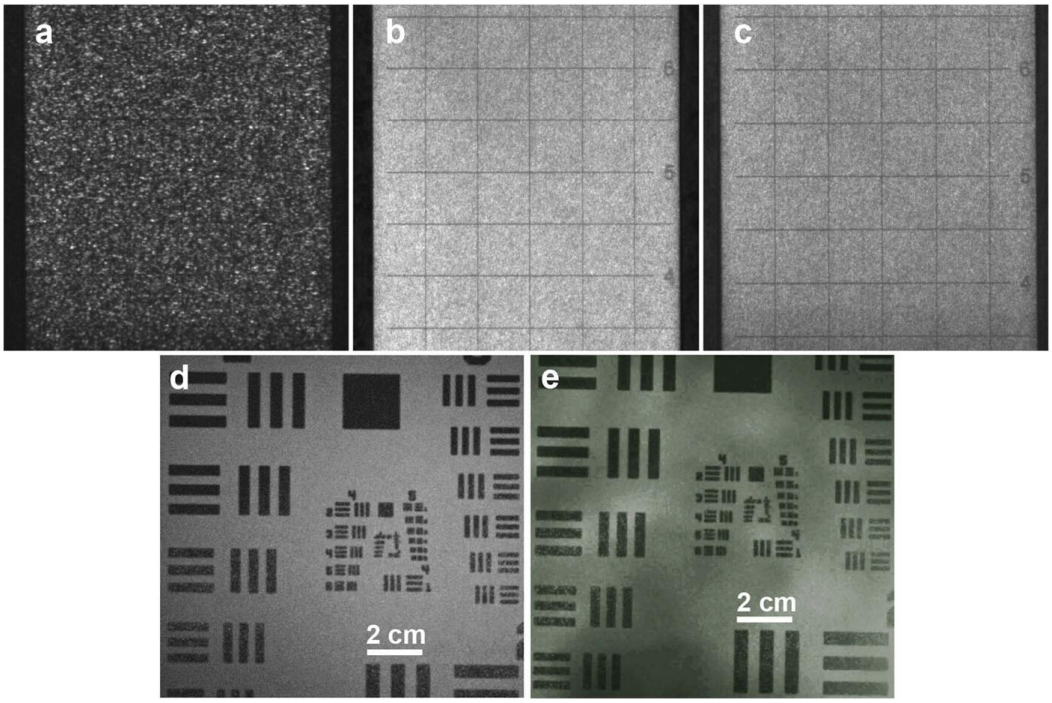

Fig. 1. (a-c) Anodized aluminum targets illuminated from semiconductor diode laser, a bare LED, and a narrow bandwidth laser array taken from 3 m. Each square is 12.7 ×12.7 mm^2. (d) and (e) were acquired with the Ti:Al_2O_3 laser from a distance of 5 m. In (e), fog was introduced in the middle of the laser and the target.

These experiments are also not limited to static objects. A video of a turbomolecular pump rotor stage was acquired while the pump was operating at 56,000 rpm. Each frame corresponds to a single laser pulse (~8 ns pulse width) of the Ti:Al_2O_3 laser cavity stabilized with the

microlens array. There is no motion blur of the rotor. A single frame is shown in Fig. 2 and the video has been published here: https://doi.org/10.1063/5.0076899.2

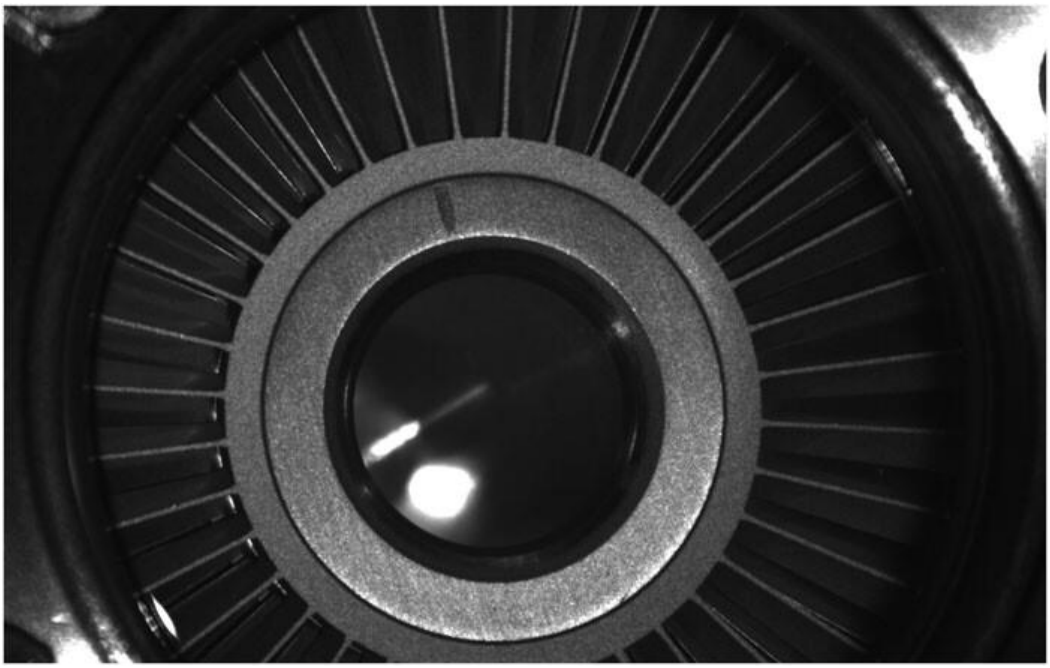

Fig. 2. One frame of a turbomolecular pump rotor stage operating with a rotational frequency of 56,000 rpm (corresponding to a velocity of 300m/s near the pump wall) acquired at a distance of 2 m with a spatial resolution of about 100 μm. The full video is available here: https://doi.org/10.1063/5.0076899.2

These results were selected from a large number of images obtained during these experiments. The specific images chosen for presentation here are, we believe, of considerable value to the Air Force because they demonstrate the feasibility of, for example, imaging the vanes of a rotor in a jet engine while the engine is in operation! It is our understanding that this is not presently possible. With this capability, however, it appears to now be possible to monitor an engine without the necessity of pulling engines from the aircraft and having them inspected visually at a Depot. Our intention is to dramatically reduce the time that an aircraft engine is out of service.

B. Biological Imaging

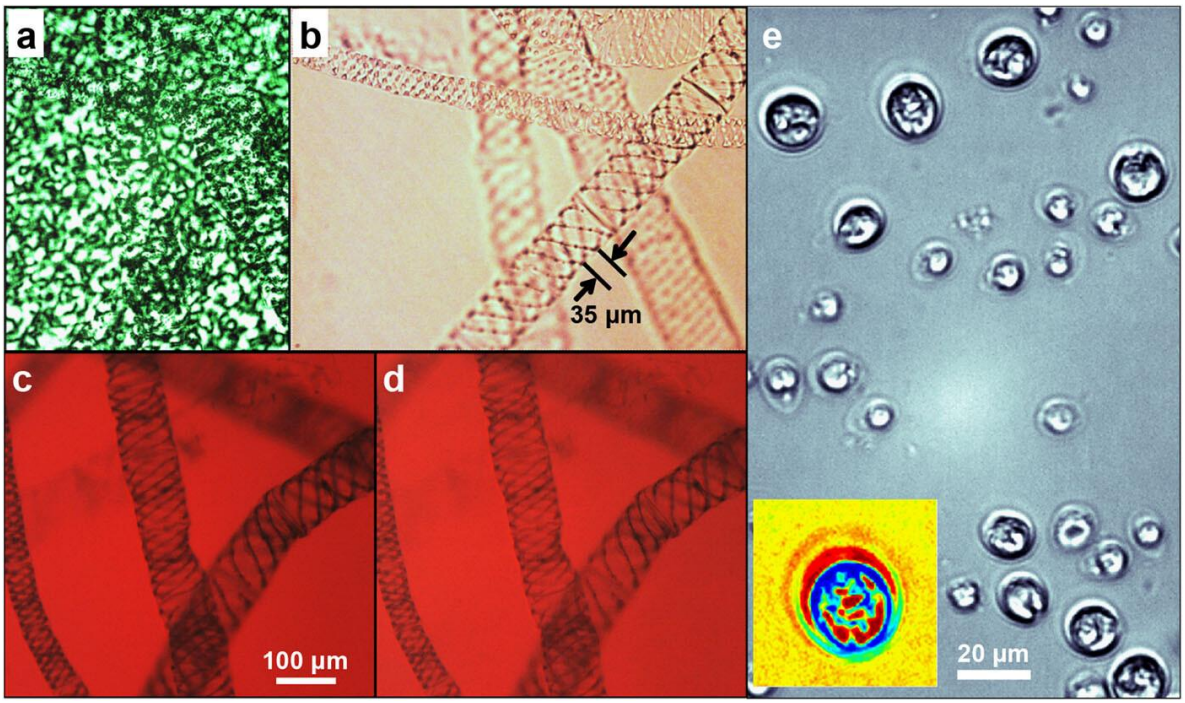

Fig. 3. Images a)-d) are of immobilized *Spirogyra* algae. a) was acquired with a 543 nm He-Ne laser at an exposure of 50 ms. b) was imaged with the Ti:Al_2O_3 microlaser pulse (1000 beams, 8 ns pulse width) c) imaged in backlit geometry with a red LED at a 50 ms exposure d) imaged with a single pulse from a red quantum dot microlaser array e) One frame of *C. reinhardtii* cells *in vivo* imaged with the Ti:Al_2O_3 microlaser pulse. Full video: https://doi.org/10.1063/5.0076899.1

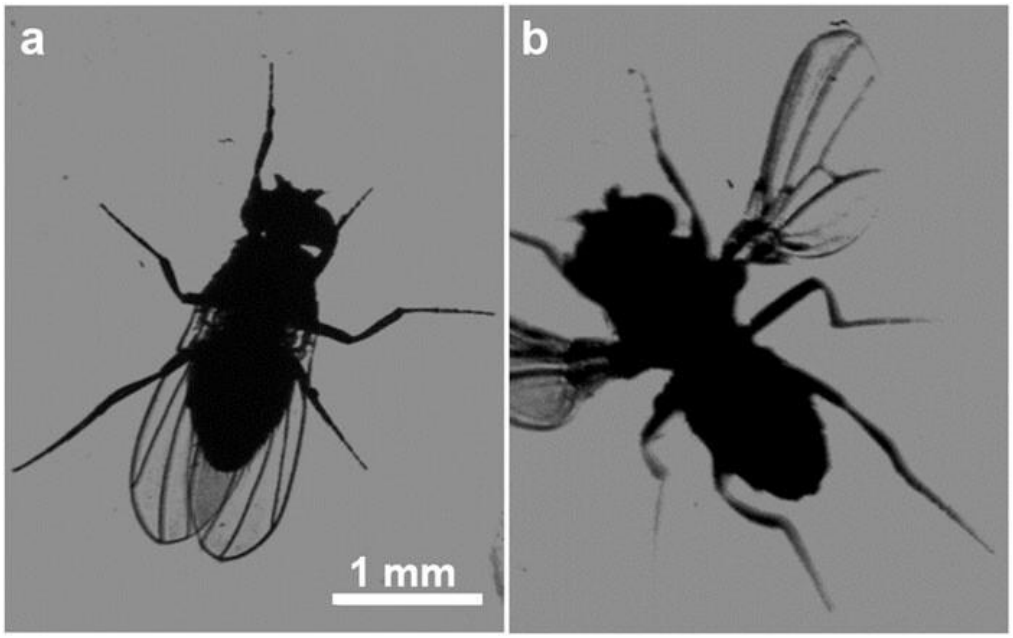

Fig. 4. Single-shot images of *Drosophila* with a spatial resolution of ~10 μm a) at rest b) in motion

The images above demonstrate the resolution in both space and time that is available with the new laser resonator conceived and developed at UIUC.

C. Fractal Lasers

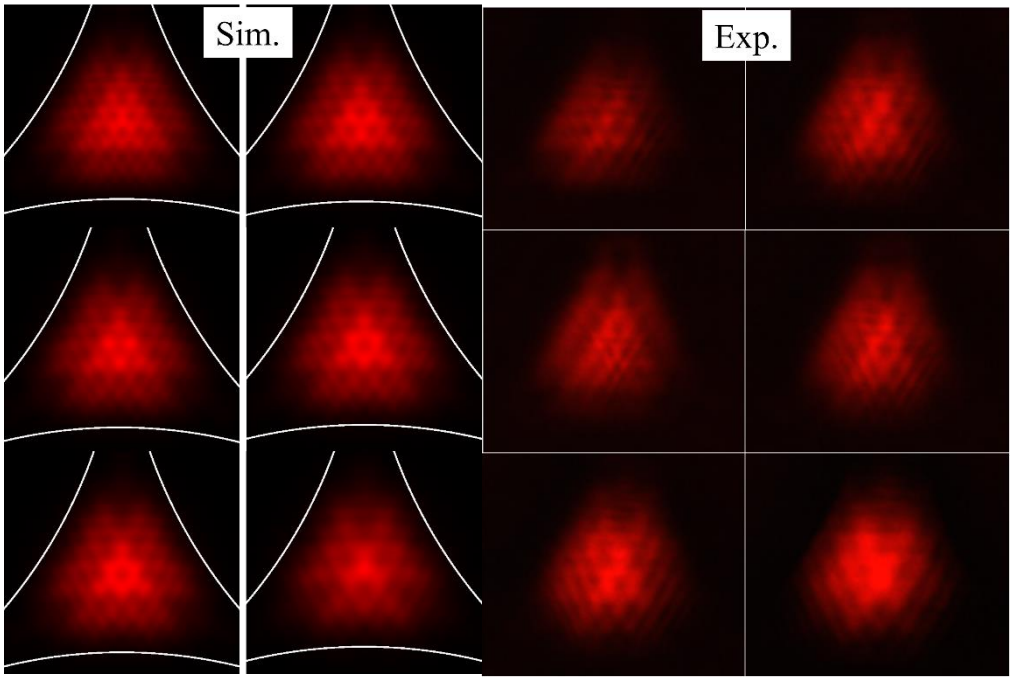

Fig. 5. Simulated and experimental intensity images of the fundamental triangular mode within different locations in the resonator starting from the bottom mirror at the upper left corner and progressively moving further away from bottom mirror. The last image is near the equator of the spheres. Each image is produced with a single pulse of the pump laser and has a resolution <2 μm.

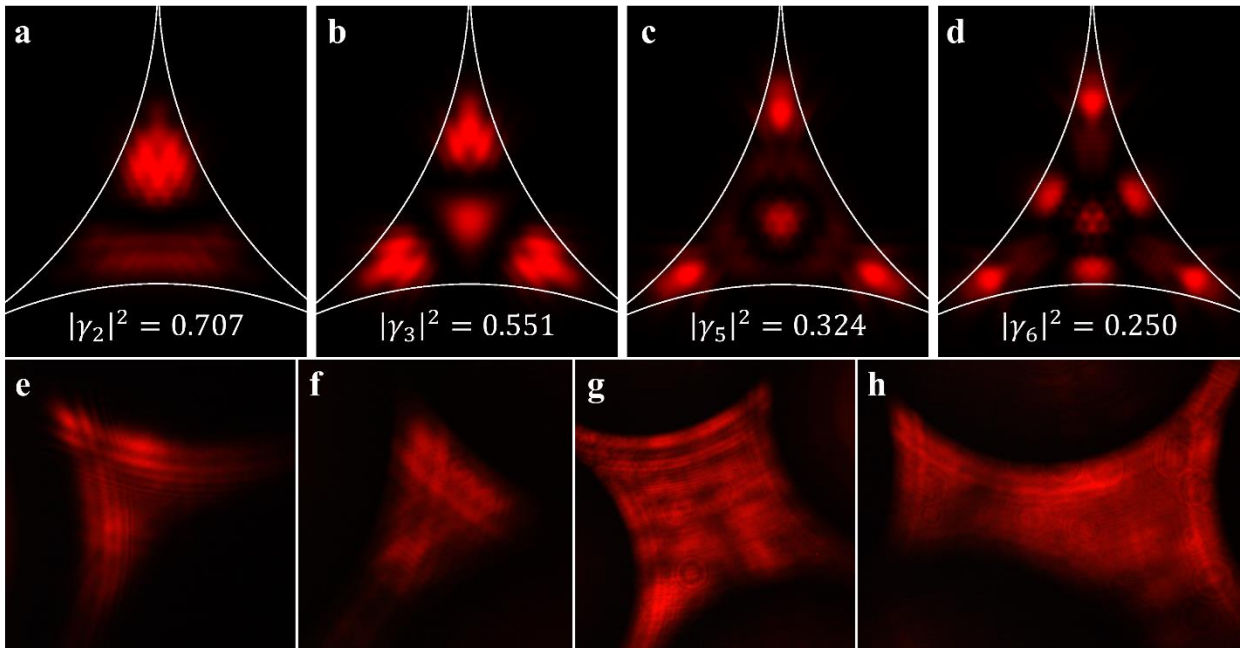

Fig. 6. Top row: Simulations for higher order fractal modes in the 3-sphere geometry at the bottom mirror along with their $|\gamma_m|^2$ value. Bottom row: experimental images obtained with a single pump pulse. The intense features of the *m*=2 and 3 fractal modes are observed.

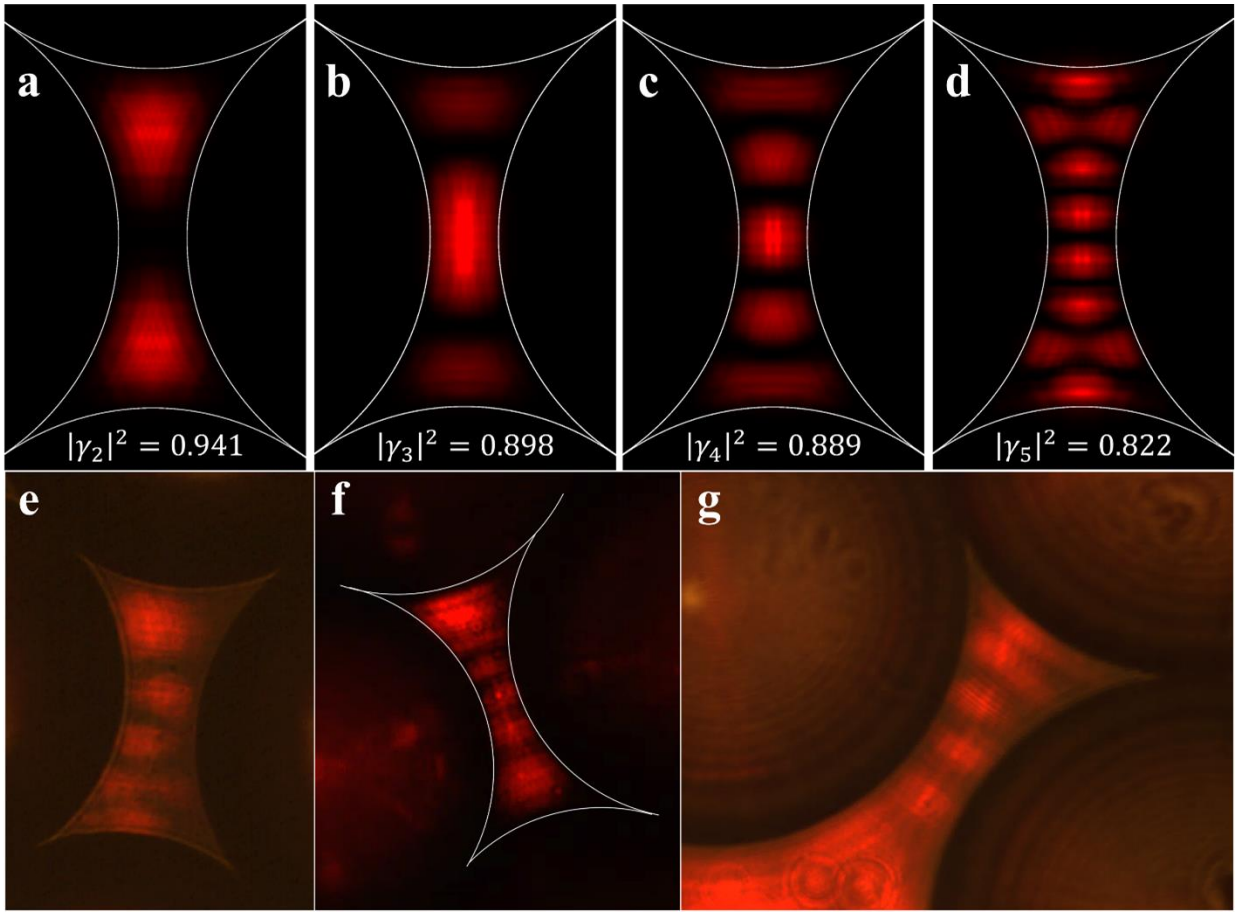

Fig. 7. Top row: simulated images for the first four high-order fractal modes from the 4-sphere arrangement along with their $|\gamma_m|^2$ values. Bottom row: experimental images of the 4-sphere modes. Panel g) is missing the bottom sphere and as a result it appears to be m=4 coupled to a continuum.

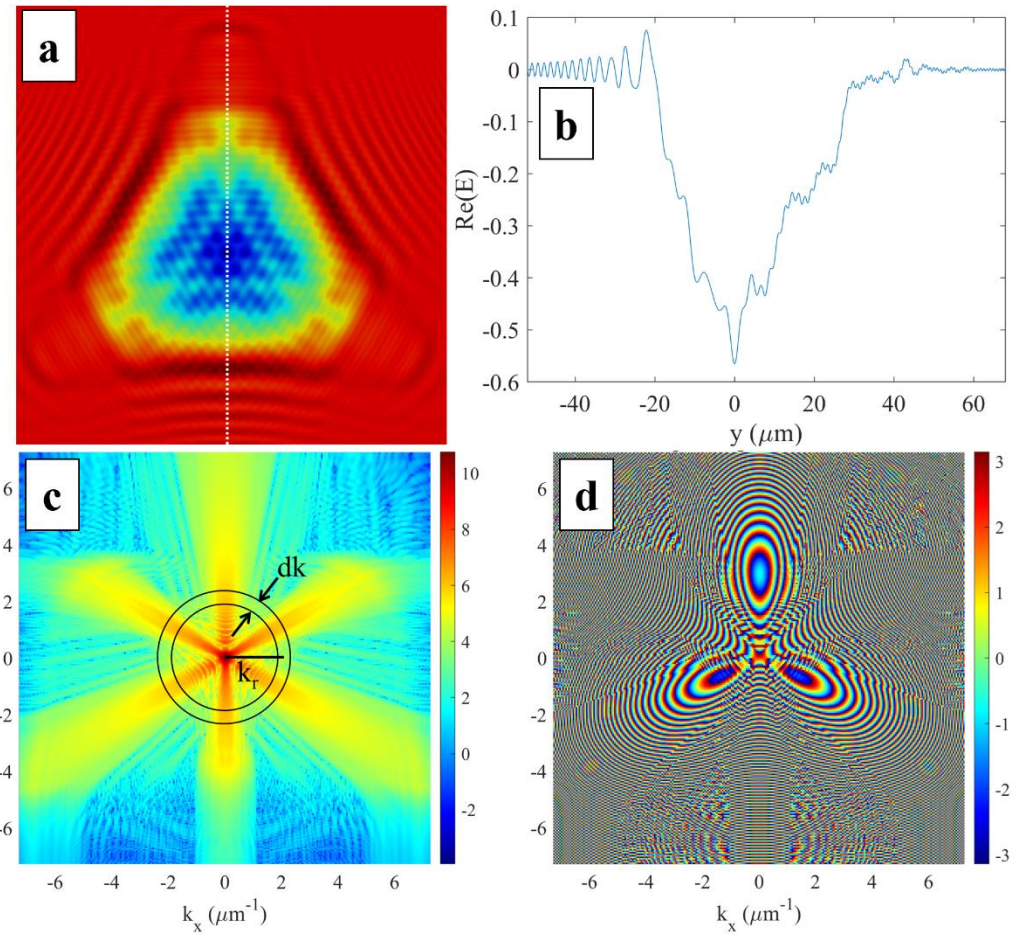

Fig. 8. Simulations for the lowest-order 3-sphere triangular mode a) false-color map of the real part of the electric field with the lineout shown in b); c) calculated angular power spectrum plotted on a log scale; d) angular spectrum phase.

As is apparent from the figures above, calculations and experiments are in agreement as to the spatial and spectral properties of these new laser modes. The advantages of these modes with regard to imaging are now under study. Also, these results are expected to be published before the end of the year.

D. Photoablative lithography at 172 nm

Precision photoablation of bulk polymers and films by microplasma-based excimer (molecular) light emitters has led to the realization of a photolithographic process in which an acrylic, polycarbonate, or other polymer serves as a dry photoresist. Patterning of the surface of commercial-grade, bulk polymers (or films spun onto Si substrates) such as poly-methyl methacrylate (PMMA) and acrylonitrile butadiene styrene (ABS) yields trenches, as well as arbitrarily-complex 3D structures, with depths reproducible to ~10 nm. Intricate patterns shown in Fig. 9 are readily produced in bulk acrylics or 40–200 nm thick acrylic films on Si with two or more exposures and overall process times of typically 10–300 s.

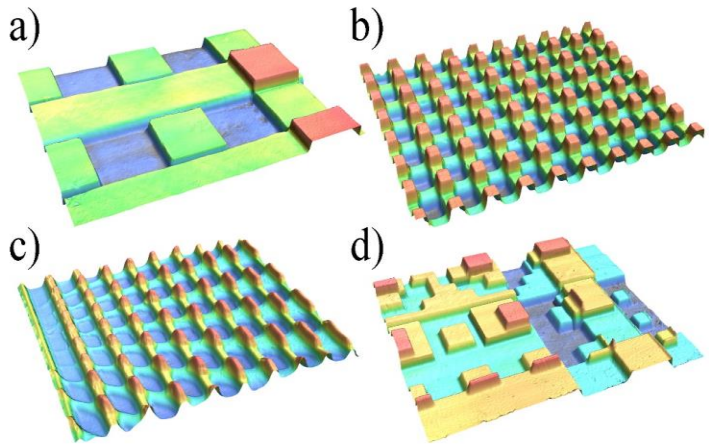

Fig. 9. False color images of several examples of nanostructures and geometries obtainable through multiple exposures of a polymer film.

Photoablation of biodegradable cellulose-base polymers, and cellulose acetate (CA) in particular, has been demonstrated recently. The process allows for simple and low-cost manufacturing of disposable microfluidic devices and optical components. In contrast to previously studied polymers such as PMMA and ABS, the CA photoetch rate does not vary with time which opens the door to an extremely powerful nanopatterning technique capable of producing >20 μm deep structures in polymers in a dry process that requires no chemicals! The demonstrated technique is environmentally friendly as no chemical waste is generated during the process. Figure 10 shows ~18 μm-deep structures produced in a commercial-grade CA as well as the floor roughness of the fabricated components. The described process was patented, and we expect that it will be used for industrial-scale manufacturing of polymer microfluidics and optics for cell phones, drones, and other imaging devices in the near future. Insofar as Air Force and DOD applications are concerned, it is now possible to inexpensively manufacture polymers "skins" for drones that have nanopatterns (gratings, phase-shift structures) designed expressly for deflecting or absorbing incoming electromagnetic signals over a broad frequency range.

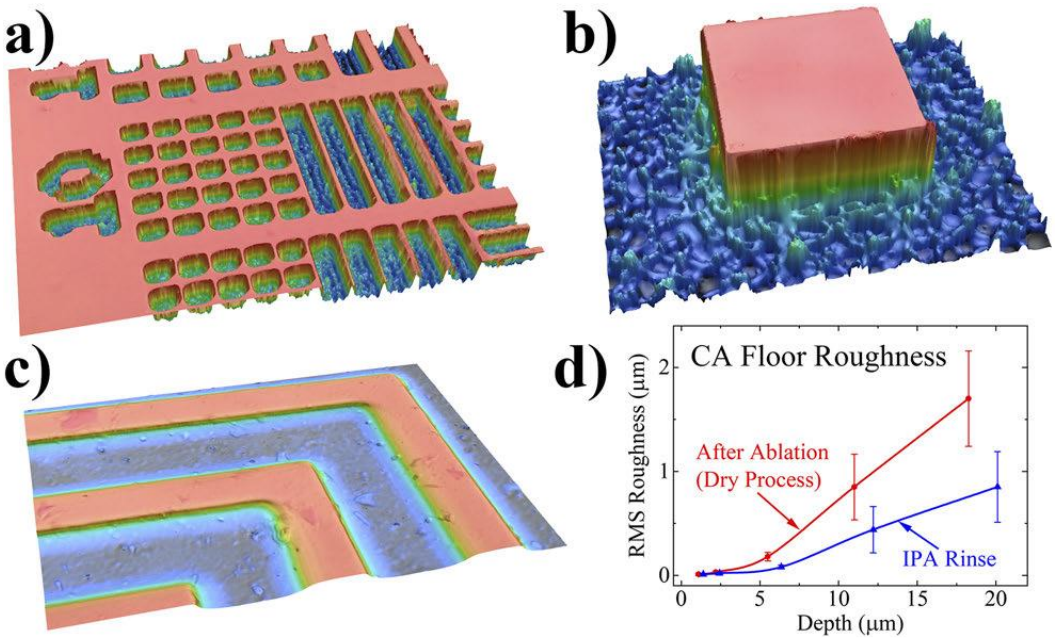

Fig. 10. Floor roughness of patterns and features etched in cellulose acetate by photoablation at 172 nm: [a), (b) False color images of lines, squares, and a mesa photoetched into commercial-grade cellulose acetate through a Cr/fused silica mask. Dimensions in the *xy* plane and along the *z* coordinate (orthogonal to, and out of, the plane) are to scale. All etched features are 21 μm in depth, and the images were recorded by laser confocal microscopy. (c) False color image of shallow trenches, 2.3 μm in depth. (d) Linear variation of the rms floor roughness with trench depth. The floor roughness (~1.75 μm for 18 μm deep trenches) for the dry process is reduced by ~50% by rinsing of the substrate in IPA. The error bars denote one standard deviation in the measurements.

E. Room Temperature Al_2O_3 Thin Film Deposition Technique

Processes for low-temperature atomic layer deposition (ALD) and etching-free film patterning have been demonstrated for Al_2O_3 thin films by dissociating the O_2 precursor in an array of microcavity plasmas. Al_2O_3 lines as narrow as 1–2 μm and ~68 nm in thickness were grown at 50°C and patterned with a conventional photoresist/*i*-line photolithography and lift-off process. Films 15–185 nm in thickness have been grown at a rate of 2.25 Å/cycle (near the theoretical limit), which remains constant up to ~700 cycles. No film growth occurs in the absence of the microplasmas, and measurements of the compositional and electrical characteristics of the Al_2O_3 films show them to be of high quality with respect to stoichiometry (O:Al ratio of 1.52), breakdown electric field strength (4.1–6.1 MV/cm), low carbon concentrations (i.e., at or below the detection limits of several analytical tools), and the virtual absence of mobile trap charge in

the oxide. These and other measurements indicate that defects in the film (as evidenced by free charge, growth rate, etc.) and the presence of impurities are minimal.

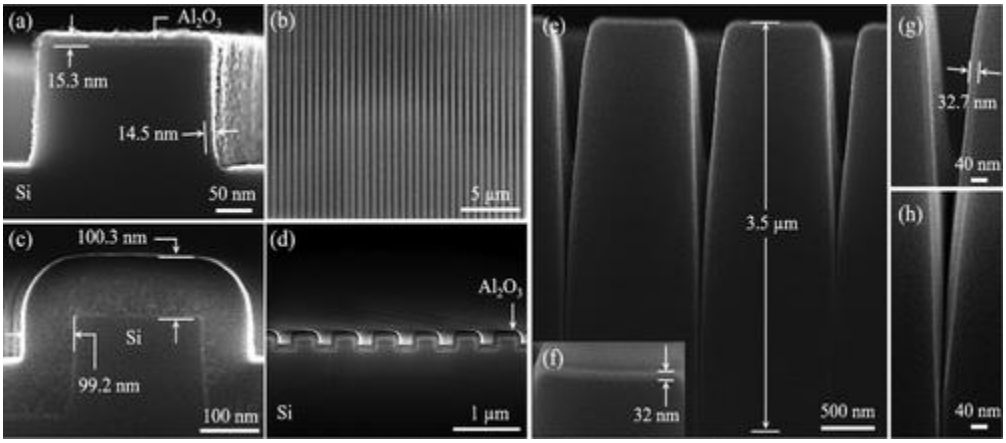

Fig. 11 Scanning electron microscopy (SEM) images of Al_2O_3 nanofilms grown onto periodic ridges and trenches in Si substrates. (a) SEM image of an ~15 nm thick Al_2O_3 film, grown onto the surface of a Si(100) wafer as well as into two adjacent trenches, and viewed slightly off the axis of the intervening ridge. (b) Panoramic view of the Al_2O_3-overcoated Si trench array of (a). (c) End-on view of a single Si ridge onto which a 100 ± 0.8 nm thick alumina film has been deposited at 50 °C by MALD. (d) Expanded portion of the Al_2O_3/Si grating of (c), also viewed off-axis to the ridges and trenches. (e) Low-resolution electron micrograph of a segment of an FIB-machined series of tapered trenches fabricated in Si. A ~33 nm thick Al_2O_3 film has been grown onto this periodic structure. (f) Expanded view of the surface of one ridge from (e), indicating the Al_2O_3 film thickness after final ion milling. (g, h) Magnified SEM views of two progressively deeper portions of one trench in (e). Note that the trench width in (h) falls below 40 nm.

The unique properties of microcavity plasmas and the confinement of the microplasma electric field within the array enclosure allow for nonequilibrium concentrations of excited atomic and molecular species to impinge on the substrate in an environment that is essentially field-free and, therefore, exempt from damage arising from ion impact at the substrate. This new plasma source permits ALD to operate at temperatures at or below those accessible in the past while eliminating damage to the films brought about by patterning with plasma etching. Consequently, films deposited by MALD may be patterned by conventional photolithography or e-beam lithography so as to have features with lateral resolution well below 300 nm. To this end, arrays and other complex geometries patterned by e-beam lithography into ~40 nm thick Al_2O_3 films have been demonstrated. Features as small as 100 nm have been observed reproducibly.

We expect that this ALD process will enable the growth of compound films, and multilayer structures, on temperature-sensitive substrates such as polymers. Furthermore, scaling of the surface area treated by MALD beyond the ~20 cm^2 value reported here is a matter only of installing multiple microplasma arrays within a processing chamber. Because of the self-

terminating nature of the ALD growth process, precision placement of the plasma arrays is unnecessary for achieving uniform growth over large areas.

Because this ALD process allows for electronic and photonic device films to be deposited at temperatures below 50 °C, such films may now (for the first time) be deposited onto flexible substrates such as polymers. Therefore, it is now possible to make polymer sheets bearing entire electronic systems that can be stretched over the surface of radomes and other antennas.

III. PAPERS PUBLISHED

The scientific articles published as a result of this AFOSR Program grant (No. FA9550-18-1-0380) are listed below. Each of them cites only AFOSR as the source of support.

1. T. C. Galvin and J. G. Eden. Markov-Airy description of optical scattering, waveguides, and resonators. *J. Opt. Soc. Am. A* **36**, 898-909 (2019).
2. A. E. Mironov, J. Kim, Y. Huang, A. W. Steinforth, D. J. Sievers, and J. G. Eden. Photolithography in the vacuum ultraviolet (172 nm) with sub-400 nm resolution: photoablative patterning of nanostructures and optical components in bulk polymers and thin films on semiconductors. *Nanoscale* (2020).
3. W. Goldshlag, R. Su, S. Park, T. O. Reboli, and J. G. Eden. Interference between atomic Rb ($5d_{5/2}$-$5p_{3/2}$) and ($5p_{3/2}$-$5s_{1/2}$) coherences: observation of an exceptional point by quantum beating at ~2.1 THz. *J. Phys. B: At. Mol. Opt. Phys.* **54**, 165001 (2021).
4. A. E. Mironov, S. Park, J. Kim, D. J. Sievers, S.-J. Park, S. Spirk, and J. G. Eden. Photoablative lithography of cellulose acetate at 172 nm: Subtractive 3D printing of biodegradable optical microstructures and molds for polydimethylsiloxane patterning. *APL Mater.* **9**, 111115 (2021).
5. J. A. Rivera, K. V. Desai, and J. G. Eden. Fluorophore-gold nanoparticle FRET/plasmonic lasers with the streptavidin-biotin complex as the acceptor-donor linkage. *AIP Adv.* **11**, 125033 (2021).
6. A. W. Steinforth, J. A. Rivera, and J. G. Eden. Imaging of transient phenomena with low coherence lasers comprising arrays of independent microbeams: A laser version of Harold Edgerton's stroboscope. *APL Photonics* **7**, 016104 (2022).
7. J.D. Hewitt, C. Campbell, K.T. Raymond, S. Park, K.V. Desai, A.E. Mironov and J.G. Eden, CsAr, CsXe, and RbXe B2Σ1/2+ Interatomic Potentials Determined from Absorption Spectra and Calculations of Franck–Condon Factors for Free–Free Optical Transitions of Atomic Collision Pairs. *Journal of Physical Chemistry* **127 (16)**, 3675 (2023).

IV. PATENTS GRANTED/SUBMITTED

1. J. G. Eden, A. Mironov, J. Kim, and D. J. Sievers. “Photoresist-free Photolithography, Photoprocessing Tools, and Methods with VUV or Deep-UV Lamp” PCT Application filed August 13, 2019.
2. J. G. Eden, A. Mironov, and D. J. Sievers. “Photoresist-Free Deposition and Patterning with Vacuum Ultraviolet Lamps”, PCT Application filed May 14, 2020

V. SELECTED CONFERENCE PRESENTATIONS

All of the conference talks listed below during this grant were supported by grant No.

1. A.W. Steinforth and J.G. Eden, “Higher-Order Fractal Laser Modes in Fabry-Pérot Resonators Containing Microspheres,” Frontiers in Optics, FW5C.3 (2021).
2. A.W. Steinforth and J.G. Eden, “Speckle-Free Imaging of Dynamic Targets without Motion Blur Using Pulse Laser Arrays,” IEEE Research and Applications of Photonics in Defense Conference, pp 1-2 (2020). *Invited Talk*
3. A.W. Steinforth and J.G. Eden, “Speckle-Free Imaging Lidar without Motion Blur using Moderate-Coherence, Nanosecond-Pulsed Lasers,” Imaging and Applied Optics, IW3B.2 (2019).